Circular Electric Wave Propagation in Periodic Structures

By G. W. LUDERER and H.-G. UNGER

(Manuscript received November 7, 1963)

TE_{01} propagation in helix waveguide and spaced-ring guide is analyzed for frequencies where the wavelength is comparable to the period of the structures. By conformal mapping the boundary value problem is reduced to that of a waveguide with smooth walls but inhomogeneous dielectric lining. The lining modifies the magnetic field near the wall and changes the distribution of eddy currents and heat losses in the wires. As frequency increases, the field penetrates more into the space between wires, the eddy currents are more evenly distributed and the heat loss decreases from its quasistatic value of, for example, 10 per cent more than in plain waveguide to only 5 per cent more. Any substantial increase in heat loss occurs only when the wavelength is shorter than the period of the structure. Due to the periodicity, there are stop-bands when any number of half wavelengths just fit into the period. The relative width of the stop-band and its maximum attenuation per period are independent of waveguide diameter and period length and are only functions of the relative geometry of the section. Because of the stop-bands being so narrow and their attenuation being quite modest, one may well accept them within the range of operating frequencies.

I. INTRODUCTION

Low-pitch helix waveguide closely wound from insulated wire has been shown to be a good transmission medium for circular electric waves.[1] Likewise, spaced-ring or spaced-disk guides have been considered for TE_{01} transmission.[2] All these structures are periodic along the axis of propagation. In analyzing them, however, the period has always been assumed short compared to the wavelength of propagation and the periodic structure then replaced by an anisotropic but homogeneous model.[3-6]

Recently, measurements have indicated that the TE_{01} loss is low

enough at very high frequencies — perhaps up to 300 gc — for the helix waveguide to be operated there.[7] At these frequencies the period could no longer be assumed to be short compared to the wavelength. Furthermore, a detailed study of the optimum jacket for most efficient unwanted mode absorption over wide frequency bands has indicated that the helix wire diameter and spacing should be nearly a third of the wavelength at the upper band limit.[8] Both these results point out the need for a more accurate analysis of circular electric wave propagation in periodic structures, taking into account a period comparable to the wavelength of propagation. It is to be expected that the distribution of electric surface currents around the helix wires or rings and disks will depend on frequency. The losses associated with these eddy currents will therefore also depend on frequency. Furthermore, a stop-band of propagation is to be expected when the wavelength becomes half the period of the structure. Both the eddy current losses and the width and height of the stop-band will be studied here.

II. MATHEMATICAL MODELS FOR PERIODIC STRUCTURES

2.1 *Spaced-Ring Guide*

Helix waveguide for TE_{01} transmission is of very low pitch. For present purposes the pitch may be neglected entirely and the helix waveguide replaced by a spaced-ring guide. Furthermore, the dielectric material in between the wires and the lossy structure surrounding the helix are of very little influence on TE_{01} propagation. They and the helix pitch may be taken into account separately.[4,6] The spaced-ring structure of Fig. 1 embedded in a homogeneous and isotropic medium will be used as a model for the present study. While this model with rings of round cross section refers in particular to helix wires of round cross section, it may readily be modified to refer to other wire cross sections or to other spaced-ring and spaced-disk guides. The general method of analysis will always be the same.

Dimensions and coordinates (x,φ,y) in Fig. 1 are chosen with respect to a mean radius a of the rings. The structure being periodic, it suffices to consider a section I/II/III/IV of the guide. Because of symmetry even only one-half (I/II′/III′/IV) of this section may be considered.

2.2 *Round Waveguide with Inhomogeneous Dielectric Lining*

2.2.1 *Maxwell's Equations*

Corresponding to a circular electric wave in round waveguide, the electromagnetic field in the spaced-ring guide will be assumed to have

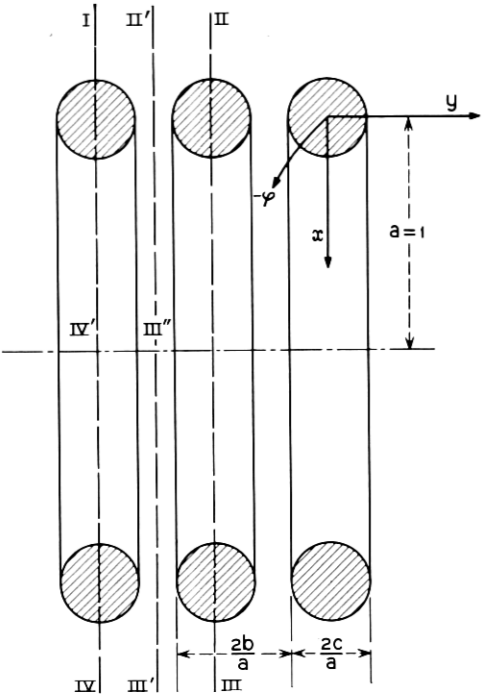

Fig. 1 — Spaced-ring guide.

only components:

$$E_\varphi , H_y , H_x .$$

For perfectly conducting rings the tangential component E_t of the electric field and normal component H_n of the magnetic field vanish on the surface of the rings

$$E_t = H_n = 0. \tag{1}$$

It is therefore expedient to use orthogonal and curvilinear coordinates which have the conducting boundaries as coordinate surfaces. Wire radius and spacing in practical structures are much smaller than the waveguide radius

$$b \ll a, \qquad c \ll a. \tag{2}$$

The curvilinear coordinates should therefore approach rectilinear coordinates as the distance from the wires increases. The coordinate $a\varphi$ may be assumed rectilinear throughout.

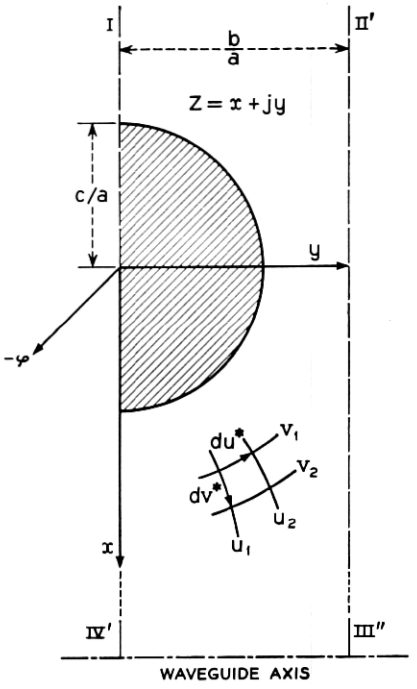

Fig. 2 — Section of spaced-ring guide in Z plane with curvilinear coordinates u and v.

Fig. 2 shows a basic section I/II′/III″/IV' of the spaced-ring line in the (x,y) plane. The curvilinear coordinates are indicated by u and v. Regarding x and y as real and imaginary coordinates in the plane of the complex variable,

$$Z = x + jy,$$

the curvilinear coordinates u and v may be regarded as real and imaginary parts of the complex variable

$$W(Z) = u(x,y) + jv(x,y). \tag{3}$$

The transition from Z to W constitutes a conformal transformation. W being an analytic function of Z, the Cauchy-Riemann equations are satisfied

$$\frac{\partial x}{\partial u} = \frac{\partial y}{\partial v}, \qquad \frac{\partial x}{\partial v} = -\frac{\partial y}{\partial u} \tag{4}$$

and the derivative may be written

$$\frac{dZ}{dW} = \frac{\partial x}{\partial u} + j\frac{\partial y}{\partial u}, \tag{5}$$

$$\left|\frac{dZ}{dW}\right| = \sqrt{\left(\frac{\partial x}{\partial u}\right)^2 + \left(\frac{\partial y}{\partial u}\right)^2} = M. \tag{6}$$

The elements of length in the Z plane of Fig. 2 are

$$du^* = \left(\frac{\partial x}{\partial u} + j\frac{\partial y}{\partial u}\right) du \tag{7}$$

$$\begin{aligned} |\, du^* \,| &= M\, du \\ |\, dv^* \,| &= M\, dv. \end{aligned} \tag{8}$$

The metrical coefficients of the curvilinear coordinates u^*, φ, v^* follow from

$$h_{v^*} = M, \qquad h_\varphi = 1, \qquad h_{u^*} = M. \tag{9}$$

Maxwell's equations written in the curvilinear system are

$$\begin{aligned} \frac{\partial}{\partial u}(E_\varphi) &= j\omega\mu_0 M H_{v^*} \\ \frac{\partial}{\partial v}(E_\varphi) &= -j\omega\mu_0 M H_{u^*} \\ \frac{\partial}{\partial u}(MH_{v^*}) - \frac{\partial}{\partial v}(MH_{u^*}) &= j\omega\epsilon_0 M^2 E_\varphi \\ \frac{\partial}{\partial v}(MH_{v^*}) + \frac{\partial}{\partial u}(MH_{u^*}) &= 0. \end{aligned} \tag{10}$$

Substituting

$$H_u = MH_{u^*}, \qquad H_v = MH_{v^*}, \qquad \epsilon = M^2(u,v) \tag{11}$$

Maxwell's equations for a fictitious W plane of rectilinear coordinates u and v obtain

$$\begin{aligned} \frac{\partial}{\partial u}(E_\varphi) &= j\omega\mu_0 H_v \\ \frac{\partial}{\partial v}(E_\varphi) &= -j\omega\mu_0 H_u \\ \frac{\partial}{\partial u}(H_v) - \frac{\partial}{\partial v}(H_u) &= j\omega\epsilon_0\epsilon E_\varphi \\ \frac{\partial}{\partial v}(H_v) + \frac{\partial}{\partial u}(H_u) &= 0. \end{aligned} \tag{12}$$

Comparing (10) and (12), the problem of finding the electromagnetic field between curved boundaries has been transformed into the problem of finding the field between straight and parallel boundaries in a medium of varying permittivity $\epsilon(u,v)$. The transition from one plane to the other ensues by conformal mapping. The analytic function of this conformal transformation by (6) and (9) determines the permittivity $\epsilon(u,v)$. This method was first developed by Routh,[9] who studied the vibration of a membrane of irregular shape by transforming it into a rectangle. The method was first applied to electromagnetic boundary value problems by Meinke[10] and Rice.[11] While in the more general field problem a fictitious inhomogeneous medium of anisotropic character has to be dealt with, at present, due to the axial symmetry $(\partial/\partial\varphi = 0)$ of the fields, the fictitious inhomogeneous medium is isotropic.

2.2.2 *Conformal Transformation*

A suitable analytic function to effect the desired transformation approximately was found by Richmond[12] and used by Morrison[13] to calculate the heat loss of circular electric waves in helix waveguide. The function is in parameter form

$$Z = \frac{2(b/a)}{\pi(1+\Psi)}\left[\tanh^{-1}\frac{\sqrt{\zeta-1}}{\sqrt{\zeta+\nu}} + \Psi\tanh^{-1}\frac{\sqrt{\zeta+1}}{\sqrt{\zeta+\nu}}\right] \tag{13}$$

$$W = \frac{b/a}{2\pi}\left[\sin^{-1}(\zeta) + \sin^{-1}\left(\frac{2\zeta+\nu-1}{\nu+1}\right)\right]. \tag{14}$$

The plane of the complex variable $Z = x + jy$ is by means of an auxiliary variable $\zeta = \xi + j\eta$ mapped onto the plane of the variable $W = u + jv$. The parameter Ψ is the smallest positive root of

$$\sin\left[\frac{\pi c}{2b}(1+\Psi)\right] = \tanh\left[\frac{\pi c}{2b}\left(1+\frac{1}{\Psi}\right)\right] \tag{15}$$

and ν is given by

$$\nu = \coth^2\left[\frac{\pi c}{2b}\left(1+\frac{1}{\Psi}\right)\right] + \cot^2\left[\frac{\pi c}{2b}(1+\Psi)\right]. \tag{16}$$

The derivative of the above analytic function is

$$\frac{dZ}{dW} = -j\frac{2}{(1+\Psi)}\frac{\sqrt{\zeta+1}+\Psi\sqrt{\zeta-1}}{\sqrt{\zeta+1}+\sqrt{\zeta+\nu}}. \tag{17}$$

The transformation of the Z plane boundaries via the ζ plane into

straight lines of the W plane is shown in Fig. 3. The waveguide radius a has been set equal to one and is the unit of length in the Z and W planes.

The transformation by (13) and (14) is only approximate and will give circular contours (D,C,B) in the Z plane only if c is somewhat smaller than b. For $c/b \rightarrow 1$ the transformation will be into a square

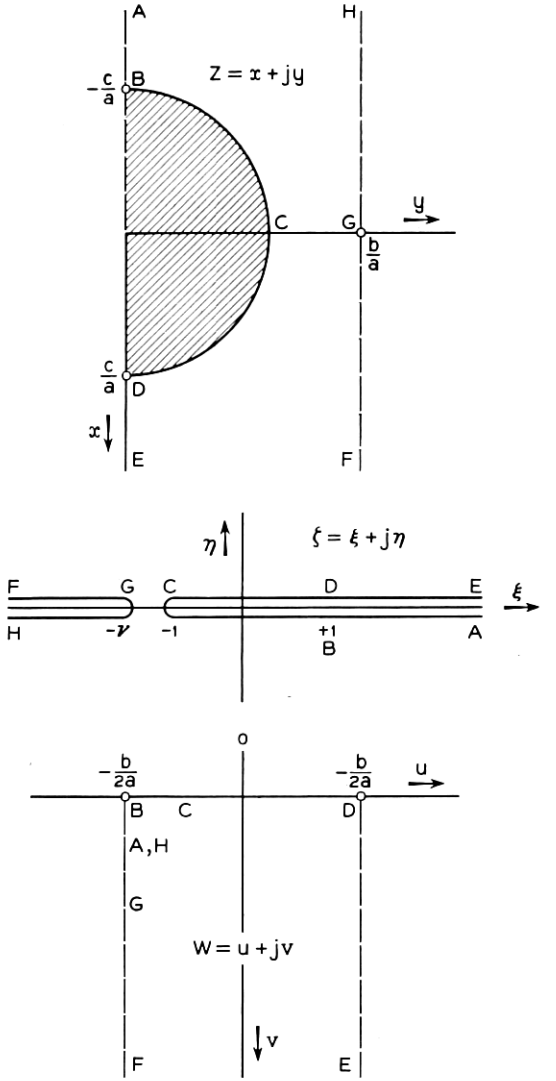

Fig. 3 — Conformal transformations by (13) and (14).

contour. For $c/b < 0.5$ the largest deviation from a circle is 2 per cent of c. In a closely wound helix the wire spacing will be determined by its insulation. Presently used helix wires have $c/b = 0.70 \cdots 0.85$. The maximum deviation from a circular radius is here between 8 and 20 per cent.

Fig. 4 shows three contours for different ratios c/b. They are obtained from (13) by letting

$$-1 \leqq \xi \leqq +1, \qquad \eta = \pm 0.$$

The resulting equations are

$$\begin{aligned} x &= \operatorname{sgn}(\eta)\, \frac{2\frac{b}{a}\Psi}{\pi(1+\Psi)} \tanh^{-1} \sqrt{\frac{\xi+1}{\xi+\nu}} \\ y &= \frac{2\frac{b}{a}}{\pi(1+\Psi)} \tan^{-1} \sqrt{\frac{1-\xi}{\nu+\xi}}. \end{aligned} \tag{18}$$

The deviations from a circular contour will be neglected subsequently.

The inverse trigonometric and hyperbolic functions in (13) and (14) are multiple valued. To obtain the rectilinear boundaries in the W plane a suitable combination of principal and other values of these functions has to be chosen (see Appendix, Section A.1).

In Fig. 5 a number of elementary cells $BDEF$ of Fig. 3 have been arranged back-to-back to form a round waveguide filled with periodically varying permittivity. The waveguide is bound by the conducting surface BCD of the rings transformed into a straight contour.

Asymptotic values of the permittivity are obtained from (17).

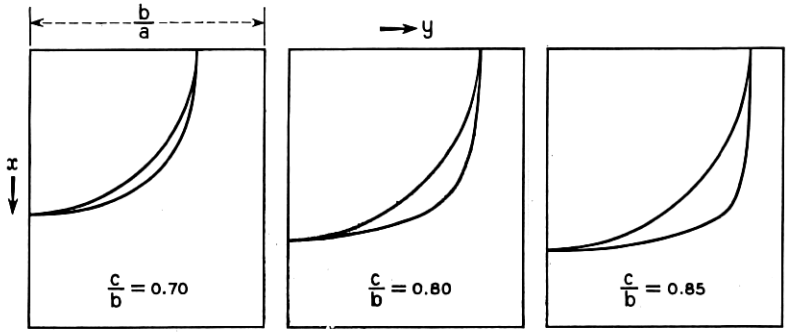

Fig. 4 — Wire contours according to (13) and (14).

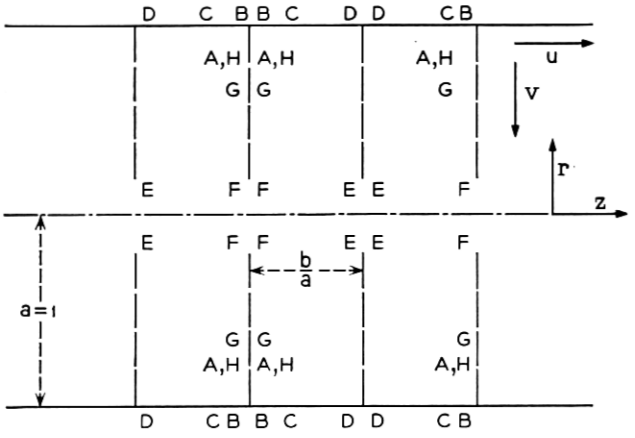

Fig. 5 — The smooth-wall waveguide formed by arranging transformed sections of Fig. 3 back-to-back.

Moving from the spaced rings towards the center of the guide:

$$\lim_{x \to +\infty} \left| \frac{dZ}{dW} \right|^2 = 1. \tag{19}$$

Moving outwardly in the opposite direction

$$\lim_{x \to -\infty} \left| \frac{dZ}{dW} \right|^2 = \infty. \tag{20}$$

According to (19), inside the guide sufficiently far from the rings, the permittivity is uniform and as in free space.

Because of (2) it differs from free space only close to the walls and may therefore be regarded as a thin dielectric lining.

According to (20), at A, H in Figs. 3 and 5 the permittivity is infinitely large. Because of (11) the region outside the rings is therefore practically free of magnetic fields.

The mathematical model thus obtained for the spaced-ring guide is a closed round waveguide with inhomogeneous dielectric lining. The permittivity of the lining may be found from (14) and (17) anywhere in the W plane.

2.3 *Approximate Model for Closed Structures*

As it is, the present model is not suitable for perturbational analysis of loss and wave interaction. Such perturbational analysis requires the relative permittivity to be distributed in the guide such that

$$\frac{1}{S}\iint_s (M^2 - 1)\, ds \ll 1$$

for any cross section. In cross sections containing the pole A,H of permittivity this condition will not be satisfied. The pole at A,H is of such a nature that not even the integral $\iint M^2\, du\, dv$ over an area in the W plane including A,H is finite.

Actually, one should expect such poles in the transformed structure. The original structure extends to infinity in cross-sectional direction. Circular electric waves in the original structure cannot be lossless normal modes but must be leaky waves, since there is some leakage of power, however small, through the gaps between the helix wires. The transformed structure, on the other hand, is bound by conducting surfaces and cannot support leaky waves.

In order to get around this difficulty and still meet the objectives of this analysis, the original structure is according to Fig. 6(a) surrounded by a magnetically conducting shield ($\epsilon = 0$, $\mu = \infty$) close to the wires. In the transformed structure of Fig. 6(b) the shield will appear as a thin wire of magnetic conductor located at A,H. This magnetic wire, being so very thin and so close to the wall, will not change the field distribution very much. It will only displace the electric field somewhat and modify the magnetic field so that it has no tangential components on its surface. For all wire spacings of practical interest this magnetic wire will be of so little influence that it may be neglected entirely and the small cross-sectional area of the wire be assumed to have $\epsilon = \mu = 1$.

The mathematical model thus obtained no longer represents the open structure of spaced wires but is an approximate representation of the magnetically closed structure. It will serve well to calculate eddy current losses and stop-bands but will not show the leakage of power through the gaps. The latter has been calculated approximately elsewhere.[3]

In all subsequent calculation the magnetic shield will be assumed at $e = b$. The corresponding small area near A,H in the transformed structure will be assumed to have $\epsilon = \mu = 1$ and will be excluded from integrations over the W plane.

III. HEAT LOSS IN HELIX WIRES

3.1 *The Magnetic Field near the Conducting Surfaces*

In round waveguide with smooth walls a dielectric lining will modify the tangential magnetic field of circular electric waves near the wall. In general, the field will be increased and will therefore add to the heat

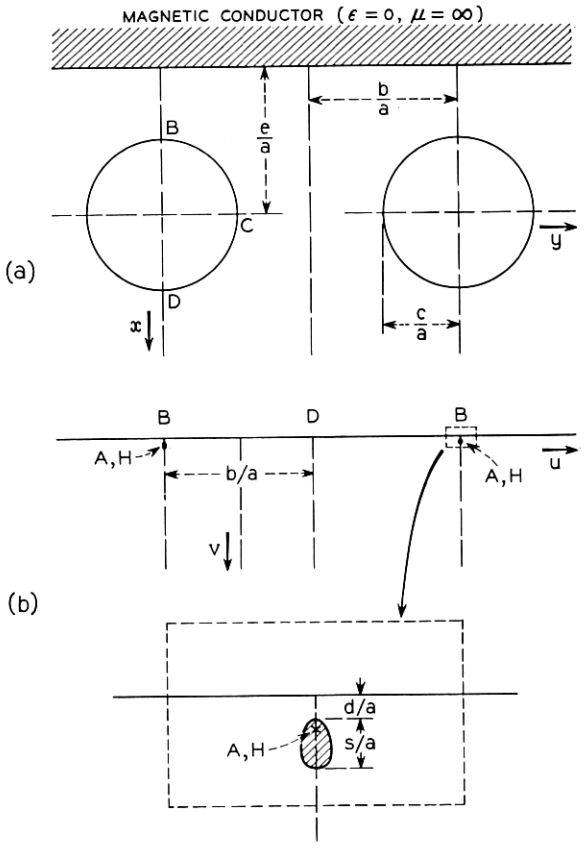

Fig. 6 — A magnetic shield (a) transformed into thin magnetic wires (b). For $c/b = 0.5$ and $e/b = 1$ the wire size is $s/b \approx 0.015$ and its distance from the wall is $d/b \approx 0.009$. For larger values of c/b, wire size and spacing decrease rapidly.

loss of circular electric waves. In helix waveguide this effect has to be taken into account in addition to the eddy current loss of the current distribution around the wire.

The change in magnetic field at the wall due to a lining, the permittivity of which is only a function of guide radius, has been calculated before[14]

$$\frac{\Delta H_u}{H_{u0}} = \omega^2 \mu_0 \epsilon_0 \int_0^a [\epsilon(r) - 1][a - r]\, dr. \tag{21}$$

H_{u0} is the longitudinal magnetic field at the smooth wall of a waveguide filled with a medium of uniform wave number $\omega\sqrt{\mu_0\epsilon_0}$. The relation may readily be generalized to take into account also a z-dependence

of permittivity (Appendix, Section A.2). Introducing the free-space wavelength

$$\lambda = \frac{2\pi}{\omega\sqrt{\mu_0\epsilon_0}}$$

and coordinates u and $v = (1/a)\ (a - r)$, the u-dependent change in magnetic field may be calculated from

$$\frac{\Delta H_u}{H_{u0}} = 4\pi^2 \left(\frac{a}{\lambda}\right)^2 \int_0^1 [M^2(u,v) - 1]v\, dv. \tag{22}$$

According to (11), the actual magnetic field H_u tangent to the conducting surfaces of the spaced-ring guide can now be written as

$$\left[\frac{H_{u^*}}{H_{u0}}\right]_{BCD} = \frac{1}{M(u,0)} \left\{1 + 4\pi^2 \left(\frac{a}{\lambda}\right)^2 \int_0^1 [M^2(u,v) - 1]v\, dv\right\} = f(u). \tag{23}$$

No closed-form solution of the integral in (23) is available. Evaluation of (23) requires (14) to be solved numerically for ξ and η. M may then be computed from (17). Representative distributions of magnetic field around the wire surface are plotted in Fig. 7. φ_w is the azimuthal angle of a slightly deformed wire cross section.

At low frequencies the space between the rings forms a waveguide below cutoff for circular electric wave fields. The magnetic field decreases rapidly with increasing φ_w. For $a/\lambda \to 0$ the quasistatic approximation obtains from (17) with

$$\frac{H_{u^*}}{H_{u0}} = \left|\frac{dW}{dZ}\right| = \left|\frac{\partial u}{\partial x} - j\frac{\partial u}{\partial y}\right| = |\ \text{grad}\ (u)\ |. \tag{24}$$

As the frequency increases the magnetic field penetrates more and more into the space between the rings. Eventually, at very high frequencies substantial circular electric wave loss will result from radiation through the rings.

3.2 *Heat Loss at High Frequencies*

Assuming the skin depth δ to be small compared to the curvature radius of a conductor surface, the power P_v lost as heat through a surface F with conductivity σ may be found from the tangential magnetic

field according to

$$P_v = \frac{1}{2\sigma\delta} \int_F | H_t |^2 \, dF. \tag{25}$$

In a waveguide section of length $2b$ and radius a with uniform magnetic field H_{u0} at the walls, the power lost as heat is

$$P_{v0} = \frac{2\pi(b/a)}{\sigma\delta} H_{u0}^2 a^2. \tag{26}$$

The power lost in one section of the spaced ring guide is

$$P_v = \frac{2\pi}{\sigma\delta} H_{u0}^2 a^2 \int_{-(b/2a)}^{+(b/2a)} \left[\frac{H_u}{H_{u0}}\right]^2 du.$$

The attenuation constant is proportional to these power losses. The ratio of attenuation due to heat loss in the spaced-ring guide to attenua-

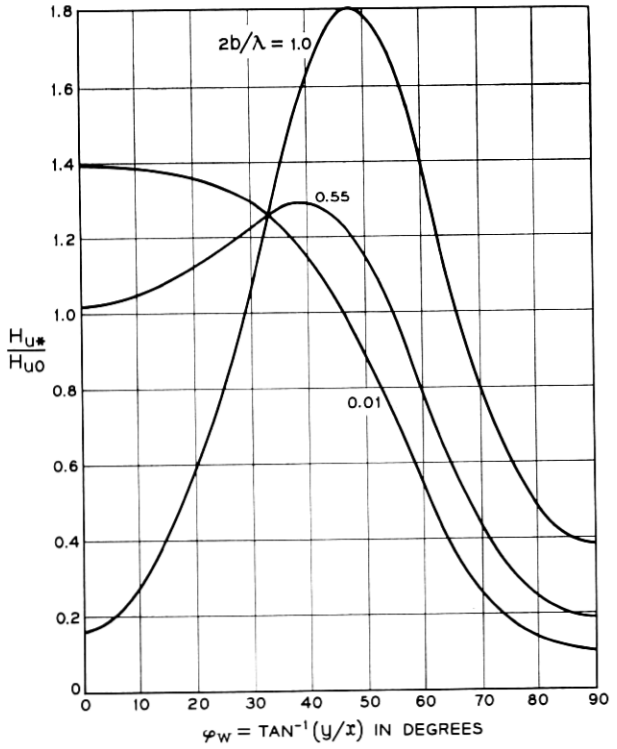

Fig. 7 — Magnetic field at the wire surface: $c/b = 0.70$.

tion in plain waveguide is therefore

$$\frac{P_v}{P_{vc}} = \frac{a}{b}\int_{-(b/2a)}^{+(b/2a)} \frac{1}{M^2}\left[1 + 4\pi^2\left(\frac{a}{\lambda}\right)^2 \int_0^1 (M^2 - 1)v\,dv\right]^2 du$$

which by substitution of $u = (b/a)\,\bar{u}$ is independent of b/a

$$\frac{P_v}{P_{v0}} = \int_{-\frac{1}{2}}^{+\frac{1}{2}} \frac{1}{M^2}\left[1 + 4\pi^2\left(\frac{a}{\lambda}\right)^2 \int_0^1 (M^2 - 1)v\,dv\right]^2 d\bar{u}. \qquad (27)$$

As in (23), no closed-form solution of the integrals is available. From a numerical evaluation of (27) representative curves of loss ratio versus frequency are plotted in Fig. 8. From its quasistatic value at low frequencies the loss ratio decreases a few per cent with increasing frequency.

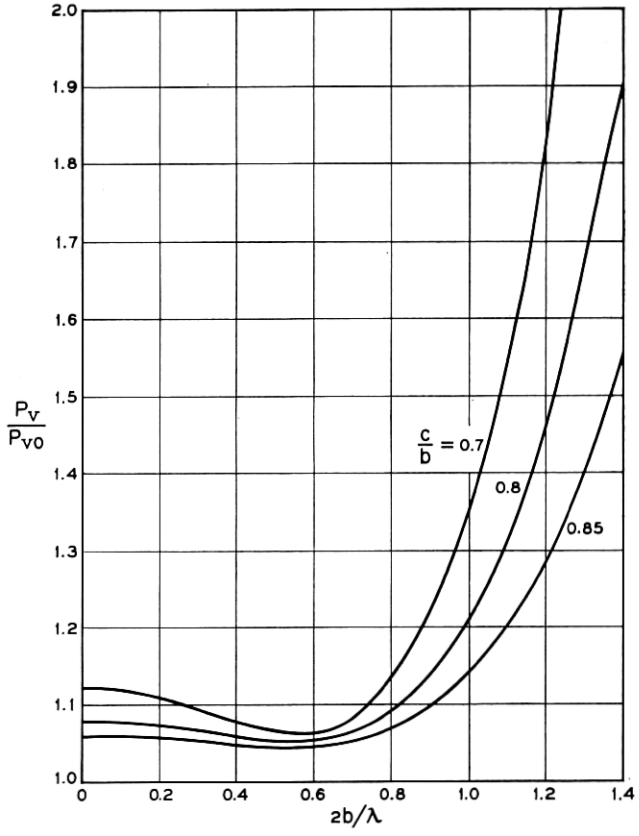

Fig. 8 — Heat loss of TE_{01} wave in helix waveguide compared to heat losses in smooth-wall waveguide.

There is a minimum of loss ratio when the free-space wavelength is nearly twice the period ($\lambda \approx 4b$). This minimum in loss ratio is due to more evenly distributed currents around the wire surface, when the magnetic field penetrates more into the space between the wires.

Any substantial increase in loss ratio will only occur when the free-space wavelength is less than the period of the structure ($\lambda < 2b$). But here the present approximations are beginning to fail.

At low frequencies for $a/\lambda \to 0$, heat loss in the quasistatic case obtains from

$$\frac{P_v}{P_{v0}} = \frac{a}{b} \int_{-(b/2a)}^{+(b/2a)} \frac{1}{M^2}\, du. \tag{28}$$

The integral in (28) has been evaluated by Morrison:[13]

$$\frac{P_v}{P_{v0}} = (1 + \Psi) \left\{ \frac{1 - \Lambda_0 (\sin^{-1} \Psi, \kappa)}{\sqrt{1 - \Psi^2}} + \cos \left[\frac{\pi c}{2b} (1 + \Psi) \right] \cot \left[\frac{\pi c}{2b} (1 + \Psi) \right] \frac{K(\kappa)}{\pi \Psi} \right\} \tag{29}$$

where

$$\kappa^2 = 1 - \frac{1}{\Psi} \cos \left[\frac{\pi c}{2b} (1 + \Psi) \right].$$

Here $K(\kappa)$ is the complete elliptic integral of the first kind and modulus κ, Λ_0 (β,κ) is Heumann's lambda function.

IV. PROPAGATION CHARACTERISTICS OF SPACED-RING SECTION

4.1 *Transmission Line Equations*

Wave propagation in the mathematical model of round waveguide with periodically inhomogeneous lining may be represented in terms of normal modes of the round waveguide without lining. The effect of the lining is to introduce coupling between these normal modes.[15]

Interaction will be strongest between those modes the beat wavelength of which is near the period of lining variations. As the frequency increases, such interaction will first occur between forward- and backward-traveling components of the circular electric wave when the guide wavelength is near twice the period length of the structure. When it is exactly twice this period length, reflections from each section will add in phase and propagation will suffer from destructive interference. Interaction with all other modes may be neglected in this range.

Coupled line equations for forward-traveling components A and backward-traveling components B of one and the same wave are written as[16]

$$\begin{aligned} \frac{dA}{dz} &= -\gamma(z)A - k(z)B \\ \frac{dB}{dz} &= k(z)A + \gamma(z)B. \end{aligned} \tag{30}$$

A and B are the amplitudes of traveling waves normalized with respect to power. $\gamma(z)$ is the propagation factor γ_0 of the wave in empty waveguide modified by the presence of the lining[5]

$$\gamma(z) = \gamma_0 - \frac{\omega^2 \mu_0 \epsilon_0 \Delta(z)}{2\gamma_c}. \tag{31}$$

$k(z)$ is the coupling or reflection coefficient between forward- and backward-traveling components of the wave[15]

$$k(z) = \frac{\omega^2 \mu_0 \epsilon_0 \Delta(z)}{2\gamma_c} \tag{32}$$

$\Delta(z)$ depends on the permittivity of the lining and its distribution over the cross section as well as on the particular wave under consideration. For TE_{01} with cylinder coordinates (r,φ,z)

$$\Delta(z) = -\int_0^a \frac{2[\epsilon_r(r,z) - 1]\, J_1^2\left(\frac{\rho_{01}}{a} r\right) r\, dr}{a^2 J_0^2(\rho_{01})}. \tag{33}$$

The relative permittivity differs from unity only close to the wall. The Bessel function in (33) may therefore be replaced by its linear approximation at its first zero ρ_{01}.

In normalized coordinates u and v, one obtains instead of (33)

$$\Delta(u) = -2\rho_{01}^2 \int_0^1 [M^2(u,v) - 1]\, v^2(1 - v)\, dv. \tag{34}$$

The coupling coefficient may now be written as

$$ak(z) = -j \frac{4\pi^2 \rho_{01}}{\frac{\lambda}{a}\sqrt{\left(\frac{2\pi}{\rho_{01}}\right)^2 - \left(\frac{\lambda}{a}\right)^2}} \int_0^1 [M^2 - 1] v^2 (1 - v)\, dv \tag{35}$$

where

$$\gamma_0^2 = \frac{\rho_{01}^2}{a^2} - \omega^2 \mu_0 \epsilon_0 \tag{36}$$

and u has been replaced by z.

Since $|k| \ll |\gamma|$ the modification of γ from (31) may be neglected in (30). Thus simplified, the transmission line equations written in matrix notation are

$$\frac{d}{dz}\begin{bmatrix} A \\ B \end{bmatrix} = \begin{bmatrix} -\gamma & -k(z) \\ k(z) & \gamma \end{bmatrix}\begin{bmatrix} A \\ B \end{bmatrix} \tag{37}$$

or

$$[A]' = [\gamma(z)] \cdot [A]. \tag{38}$$

In Fig. 9 the coupling coefficient $k(z)$ is plotted for representative values of c/b. As $c/b \to 1$ the coupling disappears because of deformation of the round wire into a square cross section by the conformal transformation.

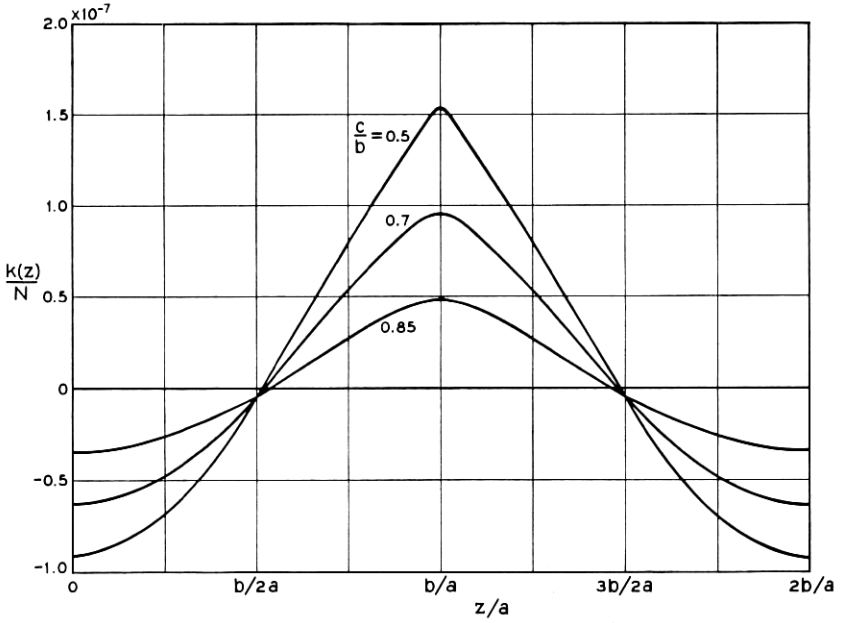

Fig. 9 — Coefficient of coupling between forward- and backward-traveling TE_{01} waves in spaced-ring waveguide.

4.2 *The Transmission Matrix*

The matrix $[\gamma(z)]$ in (38) is almost diagonal for all values of z. An approximate solution to (38) is therefore easily found by iterative integration. Thus without specifying any initial values the general transmission matrix of (38) will be calculated.

Formally integrating (38), one obtains

$$[A(l)] = [A(0)] + \int_0^l [\gamma(z)]\,[A(z)]\,dz \tag{39}$$

in form of an iterative procedure

$$[A_{\nu+1}(l)] = [A(0)] + \int_0^l [\gamma(z)]\,[A_\nu(z)]\,dz. \tag{40}$$

After two iterations, as shown in Section A.3 of the Appendix, a suitable approximation is found for the transmission matrix $[T]$ in

$$[A(l)] = [T]\cdot[A(0)]. \tag{41}$$

The elements of

$$[T] = \begin{bmatrix} T_{11} & T_{12} \\ T_{21} & T_{22} \end{bmatrix} \tag{42}$$

are

$$\begin{aligned} T_{11} &= e^{-\gamma l}\left[1 - \int_0^l k(z)\,e^{2\gamma z}\int_0^z k(z')e^{-2\gamma z'}\,dz'\,dz\right] \\ T_{12} &= -e^{-\gamma l}\int_0^l k(z)e^{2\gamma z}\,dz \\ T_{21} &= e^{\gamma l}\int_0^l k(z)e^{-2\gamma z}\,dz \\ T_{22} &= e^{\gamma l}\left[1 - \int_0^l k(z)e^{-2\gamma z}\int_0^z k(z')e^{2\gamma z'}\,dz'\,dz\right]. \end{aligned} \tag{43}$$

Substantial interaction between forward- and backward-traveling components A and B will be found only in a narrow band of frequencies centered about $\lambda = 4b$. Of all the Fourier components contained in $k(z)$, only the component k_1 of first order will contribute to the elements of the transmission matrix at frequencies near $\lambda = 4b$. Replacing $k(z)$ in (43) by this Fourier component according to

$$k(z) \approx N\, k_1 \cos\left(\frac{\pi z}{b}\right) \tag{44}$$

where

$$N = -\frac{j\, 4\pi^2\, \rho_{01}}{\lambda \sqrt{\left(\frac{2\pi}{\rho_{01}}\right)^2 - \left(\frac{\lambda}{a}\right)^2}} \tag{45}$$

is therefore indicated.

The integrals in (43) have been evaluated with this substitution and $\gamma = \alpha + j\beta$. In case of perfectly conducting walls for a period $2b$ corresponding to one section of the spaced-ring line the transmission matrix is

$$[T] \equiv \begin{bmatrix} e^{-j2\beta b}\,(1 - C_{11}) & -e^{-j2\beta b}\, C_{12} \\ e^{+j2\beta b}\, C_{21} & e^{+j2\beta b}\,(1 - C_{22}) \end{bmatrix} \tag{46}$$

where

$$\begin{aligned} C_{11} &= (e^{+j4\beta b} - 1)\left[p\,\frac{4\beta^2 b^2 + q^2}{4\beta^2 b^2 - \pi^2}\right]^2 - j\,\frac{p^2}{2\beta b}\,\frac{(4\beta^2 b^2 + q^2)^2}{(4\beta^2 b^2 - \pi^2)} \\ C_{22} &= (e^{-j4\beta b} - 1)\left[p\,\frac{4\beta^2 b^2 + q^2}{4\beta^2 b^2 - \pi^2}\right]^2 + j\,\frac{p^2}{2\beta b}\,\frac{(4\beta^2 b^2 + q^2)^2}{(4\beta^2 b^2 - \pi^2)} \\ C_{12} &= (e^{+j4\beta b} - 1)\left[p\,\frac{4\beta^2 b^2 + q^2}{4\beta^2 b^2 - \pi^2}\right] \\ C_{21} &= -(e^{-j4\beta b} - 1)\left[p\,\frac{4\beta^2 b^2 + q^2}{4\beta^2 b^2 - \pi^2}\right] \end{aligned} \tag{47}$$

$$p = -\frac{\rho_{01}^2\, k_1}{2} \tag{48}$$

$$q = 2\,\frac{b}{a}\,\rho_{01}\,. \tag{49}$$

In case of $2\beta = \pi/b$ when the section is just half the guide wavelength

$$\begin{aligned} C_{\substack{11 \\ 22}} &= -\frac{p^2}{2}\left[\frac{\pi^2 + q^2}{\pi}\right]^2 \pm j\,\frac{p^2}{4\pi}\left[\frac{\pi^2 + q^2}{\pi}\right]^2 \\ C_{\substack{12 \\ 21}} &= jp\left[\frac{\pi^2 + q^2}{\pi}\right]. \end{aligned} \tag{50}$$

4.3 *Transmission Factor*

To evaluate wave propagation in the periodic structure, its normal modes should be considered as they are composed of forward- and backward-traveling components of modes in plain guide. The normal modes propagate along the structure, changing their fields only by a constant factor from section to section. This transmission factor G of normal modes is found by looking for solutions

$$\begin{aligned} A(l) &= GA(0) \\ B(l) &= GB(0) \end{aligned} \tag{51}$$

of (41). Substituting (51) for $A(l)$ and $B(l)$ into (41), a homogeneous system of linear equations obtains which can have nontrivial solutions only for

$$\det([T] - G[U]) = 0 \tag{52}$$

where $[U]$ is the unit matrix. Values of G solving the characteristic equation (52) are

$$G_{\frac{1}{2}} = \frac{1}{2}[T_{11} + T_{22} \pm \sqrt{(T_{11} - T_{22})^2 + 4T_{12}T_{21}}]. \tag{53}$$

They are eigenvalues of the transmission matrix $[T]$ and transmission factors of normal modes of the periodic structure. Substituting from (47), (48) and (49) for the elements of $[T]$:

$$\begin{aligned} G_{\frac{1}{2}} = \cos(2\beta b) &+ 4p^2\left[\frac{4\beta^2b^2 + q^2}{4\beta^2b^2 - \pi^2}\right]^2 \sin^2(2\beta b)\cos(4\beta b) \\ &- \frac{p^2(4\beta^2b^2 + q^2)^2}{(4\beta^2b^2 - \pi^2)}\sin(2\beta b) \pm \Bigg\{4\left[p\frac{4\beta^2b^2 + q^2}{4\beta^2b^2 - \pi^2}\right]^2 \sin^2(2\beta b) \\ &- \sin^2(2\beta b) - 4\left[p\frac{4\beta^2b^2 + q^2}{4\beta^2b^2 - \pi^2}\right]^4 \sin^2(2\beta b)\cos^2(4\beta b) \\ &- \frac{p^4(4\beta^2b^2 + q^2)^4}{4\beta^2b^2(4\beta^2b^2 - \pi^2)^2}\cos^2(2\beta b) \\ &+ 4\left[p\frac{4\beta^2b^2 + q^2}{4\beta^2b^2 - \pi^2}\right]^2 \sin^2(2\beta b)\cos(4\beta b) \\ &- \frac{p^2(4\beta^2b^2 + q^2)^2}{2\beta b(4\beta^2b^2 - \pi^2)}\sin(4\beta b) \\ &+ 2\frac{p^4(4\beta^2b^2 + q^2)^4}{2\beta b(4\beta^2b^2 - \pi^2)^3}\sin(4\beta b)\cos(4\beta b)\Bigg\}^{\frac{1}{2}}. \end{aligned} \tag{54}$$

Since for $b \ll a$, $| p | \ll 1$, also, the terms of second order in p may be neglected. The transmission factors reduce to

$$G_{\frac{1}{2}} = \cos(2\beta b) \pm \left\{ 4 \left[p \frac{4\beta^2 b^2 + q^2}{4\beta^2 b^2 - \pi^2} \right]^2 \sin^2(2\beta b) + 4 \left[p \frac{4\beta^2 b^2 + q^2}{4\beta^2 b^2 - \pi^2} \right]^2 \sin^2(2\beta b) \cos(4\beta b) - \frac{p^2 (4\beta^2 b^2 + q^2)^2}{2\beta b (4\beta^2 b^2 - \pi^2)} \sin(4\beta b) \right\}^{\frac{1}{2}}. \tag{55}$$

In case of $2\beta b = \pi$:

$$\begin{aligned} G_{\frac{1}{2}} &= -1 \mp p \left(\pi + \frac{q^2}{\pi} \right) \\ &= -1 \pm \frac{k_1 \pi \rho_{01}^2}{2} \pm \frac{2k_1 \left(\frac{b}{a} \right)^2 \rho_{01}^4}{\pi}. \end{aligned} \tag{56}$$

4.4 *Evaluation of the Transmission Factor*

Writing $G = e^{-\gamma' l}$, attenuation factor

$$2\alpha' b = \ln | G | \tag{57}$$

and phase factor

$$2\beta' b = \sphericalangle G \tag{58}$$

of one section of a spaced-ring guide obtain.

Frequency ranges for which G is real constitute stop-bands of the periodic structure. There is no phase change from section to section in stop-bands, but only a decrease in amplitude by G. Stop-bands are characterized by a positive quantity under the square root of (55). Outside of stop-bands this quantity is negative. The stop-bands extend to the zeros of the square root.

Since $| p | \ll 1$, the square root will be zero only when $| \sin 2\beta b | \ll 1$ also; letting $2\beta b = \pi - \theta$ with $| \theta | \ll 1$, (55) may be approximated near the stop-band by

$$G_{\frac{1}{2}} \approx -1 \pm \sqrt{p^2 \pi^2 - \theta^2}. \tag{59}$$

Within the stop-band for

$$| \theta | < | p\pi | = \left| \frac{\rho_{01}^2 k_1 \pi}{2} \right|$$

the attenuation constant is:

$$\alpha' a = \frac{a}{2b} \sqrt{\left(\frac{\rho_{01}^2 k_1}{2}\right)^2 - \theta^2}.$$

With

$$2\beta b \approx 4\pi \frac{b/a}{\lambda/a}$$

for waves sufficiently far from cutoff, the deviation θ from the half-wavelength condition may be expressed by

$$\theta = \pi\left(1 - \frac{4b}{\lambda}\right)$$

and the attenuation constant be written

$$\alpha' a = \frac{a}{2b} \sqrt{\left(\frac{\rho_{01}^2 k_1 \pi}{2}\right)^2 - \pi^2\left(1 - \frac{4b}{\lambda}\right)^2}. \tag{60}$$

For $\theta = 0$ the center frequency of the stop-band obtains, corresponding to

$$\begin{aligned} \frac{a}{\lambda} &= \sqrt{\left(\frac{a}{4b}\right)^2 + \left(\frac{\rho_{01}}{2\pi}\right)^2} \\ &\approx \frac{a}{4b} \quad \text{when} \quad \frac{b}{a} \ll 1. \end{aligned} \tag{61}$$

Here the attenuation constant is

$$\alpha' a = \frac{\rho_{01}^2 k_1 \pi a}{4b/a}. \tag{62}$$

With $\theta = \pm(\rho_{01}^2 k_1 \pi)/2$, for the stop-band limits the relative width of the stop-band is

$$\frac{\Delta\omega}{\omega} = \rho_{01}^2 k_1. \tag{63}$$

In the present approximation, neglecting heat losses in the conductors, there is no attenuation outside of stop-bands.

Taking these heat losses into account, $2\beta b$ in (55) has to be replaced by $2\beta b - j2\alpha b$, where

$$\alpha = \alpha_{01} \frac{P_v}{P_{v0}}$$

according to Section II. Since $2\alpha b \ll 1$, the attenuation constant at

the center of the stop-band is in this case

$$\alpha' a = \frac{\rho_{01}^2 k_1(\pi - 4\alpha b)a}{4b/a}. \tag{64}$$

The numerical evaluations in Section II and plots of Fig. 8 show $\alpha \approx \alpha_{01}$ well beyond the first stop-band. Since $4\alpha b \ll \pi$ also the stop-band attenuation and width will not be affected noticeably by the finite conductivity of the wires.

For numerical evaluation of stop-band attenuation and width the Fourier coefficient k_1 according to (44) has been computed and plotted in Fig. 10 versus c/b. k_1 is larger the smaller the ratio c/b. For $c \to b$ the present conformal transformation is into square wires without spaces. In this case $k_1 \to 0$. But for $c/b < 0.80$ the approximation of round wires is satisfactory.

Stop-band attenuation $2\alpha' b$ per section and relative stop-band width $\Delta\omega/\omega$ according to (62) and (63) are both proportional to k_1. Fig. 10 has therefore been provided with additional scales to also represent these two quantities as a function of c/b.

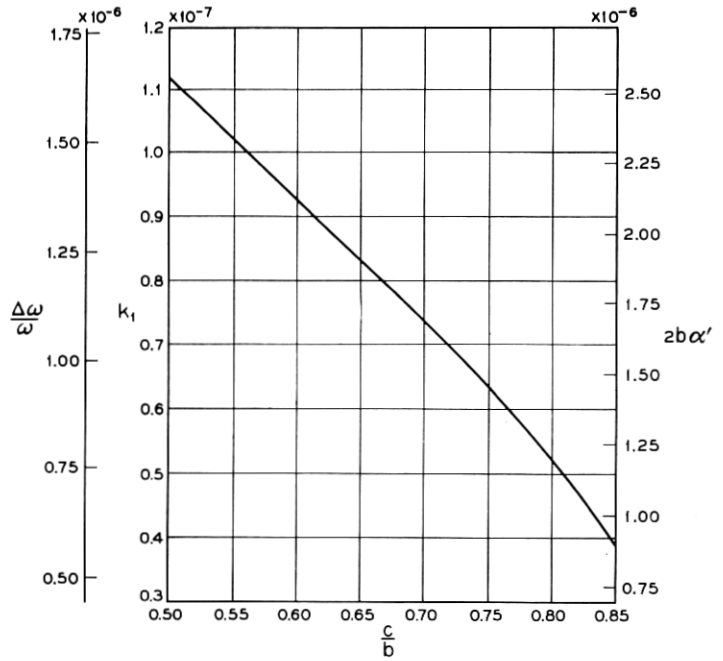

Fig. 10 — First-order Fourier coefficient of TE_{01} coupling in spaced-ring guide; additional scales indicate stop-band width and attenuation.

It is most important for practical purposes that the stop-band attenuation reach only quite modest values and that the stop-band be very narrow. $2\alpha' b$ and $\Delta\omega/\omega$ being only functions of c/b, the absolute quantities α' and $\Delta\omega$ of the stop-band will both be smaller the larger the length $2b$ of the section, provided of course one stays within the range where present approximations hold.

Take for example a helix wire spaced by $2b = 0.15$ mm with $c/b = 0.75$, corresponding to present design practices.[17] The stop-band would occur at $\lambda = 0.3$ mm, corresponding to $f = 1000$ gc. The width $\Delta f = 925$ kc and attenuation $\alpha' = 35$ db/mile of the stop-band would not be objectionable because it is well beyond the frequency range where the helix waveguide will be operated.

Helix wires spaced by $2b = 0.3$ mm with $c/b = 0.75$ corresponding to an optimum design for wideband unwanted mode absorption[8] would have a stop-band at 500 gc of width $\Delta f = 462.5$ kc and attenuation $\alpha' = 67$ db/mile. Both quantities are smaller but also not objectionable since still outside the operating range.

If, however, no other limitation is imposed on the wire geometry but the space between to be cutoff for circular electric wave fields at the highest operating frequency, then with $c/b = 0.75$ and $\epsilon_r = 3$ for the space between wires:

$$2(b - c) < \frac{1}{2\sqrt{\epsilon_r}} \lambda_{\min}$$

$$2b < \frac{2}{\sqrt{\epsilon_r}} \lambda_{\min}$$

To utilize the full range of mm-waves $\lambda_{\min} = 1$ mm. Then $2b = 1$ mm will keep the space between wires sufficiently below cutoff.

The stop-band will now occur within the operating range at $f = 150$ gc but it will only be $\Delta f = 139$ kc wide and have the attenuation $\alpha' = 20$ db/mile. Both values are small enough not to be objectionable.

V. CONCLUSIONS

Helix waveguide, spaced-ring or spaced-disk guides or other periodic structures for circular electric wave transmission may well be operated close to or beyond the frequency where the wavelength of propagation is twice the period of the structure. The nonuniform but periodic structure of the conducting boundaries in such waveguides will cause an increase in wall current losses due to nonuniform distribution of the eddy currents. From its quasistatic value at low frequencies this distri-

bution will become more even as the frequency increases and the magnetic field penetrates more into the grooves or spaces between wires, rings or disks. The relative loss with respect to smooth wall guide will thus decrease by up to 5 per cent before it shows any substantial increase when the wavelength of propagation becomes smaller than the period of the structure.

The periodic structure causes a stop-band in circular electric wave transmission, when the wavelength of propagation is twice the period length. The stop-band attenuation is, however, quite modest and, what is even more important, the stop-band is very narrow. The relative width of the stop-band and the stop-band attenuation per section are independent of waveguide size and frequency and are functions only of the ratio of wire size to wire spacing or of corresponding dimensionless factors describing the geometry. Deviating from present design practices, one may therefore make the structure of relatively large period, accepting a very narrow stop-band within the operating range. In 2-inch I.D. helix waveguide of optimum design for unwanted mode absorption the wire size is $2c = 0.225$ mm and wire spacing $2b = 0.300$ mm. The stop-band occurs near 500 gc; its width is $\Delta f = 462.5$ kc and maximum attenuation $\alpha' = 67$ db/mile. Keeping the ratio $c/b = 0.75$ the same, but increasing the spacing to $2b = 1$ mm, the stop-band will occur at 150 gc but will be only 139 kc wide and have a maximum attenuation of 20 db/mile.

APPENDIX

A.1 *Conformal Transformation*

Parameter Ψ of the transformation was found for several values of c/b by solving (15) numerically using Newton's formula. Subsequently ν was calculated from (16). Both quantities are listed in Table I. Also listed in this table for all values of c/b is the largest deviation of the

TABLE I

c/b	Ψ	ν	r_{max}/c	P_v/P_{v0}
0,5	0.653 257 600 1	1.155 982 500	1.018	1.225
0,6	0.528 077 816 1	1.034 531 436	1.039	1.170
0,7	0.391 940 793 8	1.003 248 064	1.078	1.126
0,8	0.247 192 783 0	1.000 024 889	1.149	1.082
0,85	0.176 268 291 6	1.000 000 146	1.199	1.060

contour DCB in Fig. 3 from a circle as it is found from (18) and

$$\frac{r_{\max}}{c} = \left[\sqrt{\left[\frac{x}{(c/b)(b/a)}\right]^2 + \left[\frac{y}{(c/b)(b/a)}\right]^2}\right]_{\max}. \tag{65}$$

For further reference the loss ratio P_v/P_0 in the quasistatic case according to (29) is likewise listed in Table I.

The area in the Z plane to be mapped on to the W plane is multiple-connected. Hence care has to be taken to select suitable values of the multiple-valued functions in (13) and (14). From (14)

$$\frac{2\pi a}{b}(u + jv) = \sin^{-1}(\zeta) + \sin^{-1}(\chi) \tag{66}$$

$$\chi = \frac{2\zeta + \nu - 1}{\nu + 1}. \tag{67}$$

To obtain rectilinear boundaries in the W plane, principal and other values of $\sin^{-1}\zeta$ and $\sin^{-1}\chi$ must be combined. Suitable combinations are listed in Table II.

TABLE II

Phase range of	$X = \text{Re}\,[\sin^{-1}(\zeta)]$	$Y = \text{Im}\,[\sin^{-1}(\zeta)]$
$0 < \sphericalangle\zeta < \pi/2$	$\pi/2 > X > 0$	$Y > 0$
$\pi/2 < \sphericalangle\zeta < \pi$	$0 > X > -\pi/2$	$Y > 0$
$-\pi/2 < \sphericalangle\zeta < 0$	$\pi > X > \pi/2$	$Y > 0$
$-\pi < \sphericalangle\zeta < -\pi/2$	$3\pi/2 > X > \pi$	$Y > 0$
	$X = \text{Re}\,[\sin^{-1}(\chi)]$	$Y = \text{Im}\,[\sin^{-1}(\chi)]$
$0 < \sphericalangle\chi < \pi/2$	$\pi/2 > X > 0$	$Y > 0$
$\pi/2 < \sphericalangle\chi < \pi$	$0 > X > -\pi/2$	$Y > 0$
$-\pi/2 < \sphericalangle\chi < 0$	$-2\pi < X < -3\pi/2$	$Y < 0$
$-\pi < \sphericalangle\chi < -\pi/2$	$-5\pi/2 < X < -2\pi$	$Y < 0$

Of the inverse hyperbolic functions in (13) the principal value is used throughout, but both values of the square roots of the arguments are taken alternatively.

Likewise, suitable values of the square roots in the derivative (17) must be selected as well as in

$$\frac{dZ}{d\zeta} = \frac{b/a}{\pi(1 + \Psi)}\left[\frac{1}{\sqrt{\zeta - 1}\cdot\sqrt{\zeta + \nu}} + \frac{\Psi}{\sqrt{\zeta + 1}\cdot\sqrt{\zeta + \nu}}\right] \tag{68}$$

and

$$\frac{dW}{d\zeta} = j\,\frac{b/a}{2\pi}\left[\frac{1}{\sqrt{\zeta - 1}\cdot\sqrt{\zeta + \nu}} + \frac{1}{\sqrt{\zeta + 1}\cdot\sqrt{\zeta - 1}}\right] \tag{69}$$

where $\zeta = \xi + j\eta$, which are subsequently used in numerically solving (13) and (14).

Since only areas of the Z plane with $y \geqq 0$ are being mapped, the square roots $\sqrt{\zeta - 1}$ and $\sqrt{\zeta + \nu}$ in $Z(\zeta)$ according to (13) must be chosen of equal sign in case of $\eta \geqq 0$ and opposite sign in case of $\eta < 0$. This choice will insure the proper asymptotic values of $|\, dZ/dW \,|^2$ in (19) and (20).

A.2 *Magnetic Field and Wall Current of Circular Electric Waves in Lined Waveguide*

From Maxwell's equations in cylindrical coordinates

$$\frac{\partial H_r}{\partial z} - \frac{\partial H_z}{\partial r} = j\omega\epsilon\epsilon_0 E_\varphi .$$

For the difference of magnetic field $\Delta H = H - H_0$ in lined waveguide and empty waveguide

$$\frac{\partial \Delta H_z}{\partial r} = -j\omega\epsilon_0(\epsilon E_\varphi - E_{\varphi 0}) + \frac{\partial \Delta H_r}{\partial z} \tag{70}$$

may be written.

The radial component H_r of magnetic field vanishes at the wall; close to the wall it is small. In order to find the change in magnetic field at the wall due to a thin lining (70) may be approximated by

$$\frac{\partial \Delta H_z}{\partial r} = -j\omega(\epsilon - 1)\epsilon_0 E_{\varphi 0} \tag{71}$$

and the change in magnetic field at the wall calculated from the relative permittivity $\epsilon(r,z)$ and the electric field

$$E_{\varphi 0} = jA\mu_0\omega\rho_{01}J_0'(\rho_{01}r)e^{-\gamma z} \tag{72}$$

of a circular electric wave in empty guide.

Substituting for $E_{\varphi 0}$ from (72) into (71) and integrating

$$\Delta H_z = A\omega^2\mu_0\epsilon_0 \int_0^a (\epsilon - 1)\rho_{01}J_0'(\rho_{01}r)\, dr\, e^{-\gamma z}. \tag{73}$$

For a thin lining

$$\Delta H_z = A\omega^2\mu_0\epsilon_0\rho_{01}^2 J_0(\rho_{01}a) \int_0^a (\epsilon - 1)(a - r)\, dr\, e^{-\gamma z} \tag{74}$$

which, when compared to the magnetic field

$$H_{z0} = A\rho_{01}^2 J_0(\rho_{01} r)\, e^{-\gamma z}$$

at the wall of the empty guide, gives

$$\frac{\Delta H_z}{H_{z0}} = \omega^2 \mu_0 \epsilon_0 \int_0^a (\epsilon - 1)(a - r)\, dr.$$

The relative change in wall current is given by the same expression.

A.3 *Integration of Coupled Line Equations*

By substituting

$$\begin{aligned} A &= ve^{-\gamma z}, \quad A(0) = v(0), \quad A(l) = v(l)e^{-\gamma l} \\ B &= we^{\gamma z}, \quad B(0) = w(0), \quad B(l) = u(l)e^{\gamma l} \end{aligned} \tag{75}$$

for A and B in (37) the following system of equations for v and w obtains:

$$\frac{d}{dz}\begin{bmatrix} v(z) \\ w(z) \end{bmatrix} = \begin{bmatrix} 0 & -ke^{2\gamma z} \\ ke^{-2\gamma z} & 0 \end{bmatrix} \cdot \begin{bmatrix} v(0) \\ w(0) \end{bmatrix}. \tag{76}$$

Integrating according to the procedure (40), the first-order approximation to a solution is

$$\begin{bmatrix} v(z) \\ w(z) \end{bmatrix} = \begin{bmatrix} 1 & -\int_0^z ke^{2\gamma z}\, dz \\ \int_0^z ke^{-2\gamma z}\, dz & 1 \end{bmatrix} \cdot \begin{bmatrix} v(0) \\ w(0) \end{bmatrix}. \tag{77}$$

Another iteration results in the second-order solution

$$\begin{bmatrix} v(z) \\ w(z) \end{bmatrix} = \begin{bmatrix} 1 - \int_0^z ke^{2\gamma z} \int_0^z ke^{-2\gamma z'}\, dz'dz & \vdots & -\int_0^z ke^{2\gamma z}\, dz \\ \int_0^z ke^{-2\gamma z}\, dz & \vdots & 1 - \int_0^z ke^{-2\gamma z} \int_0^z ke^{2\gamma z'}\, dz'dz \end{bmatrix} \cdot \begin{bmatrix} v(0) \\ w(0) \end{bmatrix} \tag{78}$$

which is adequate for present purposes. Replacing v and w by A and B, the transmission matrix is contained in

$$\begin{bmatrix} A(l) \\ B(l) \end{bmatrix} = \begin{bmatrix} \left[1 - \int_0^l ke^{2\gamma z} \int_0^z ke^{-2\gamma z'}\, dz'dz\right] e^{-\gamma l} & \vdots & -\int_0^l ke^{2\gamma z}\, dz\, e^{-\gamma l} \\ \int_0^l ke^{-2\gamma z}\, dz\, e^{\gamma l} & \vdots & \left[1 - \int_0^l ke^{-2\gamma z} \int_0^z ke^{2\gamma z'}\, dz'dz\right] e^{\gamma l} \end{bmatrix} \cdot \begin{bmatrix} A(0) \\ B(0) \end{bmatrix}.$$

REFERENCES

1. Morgan, S. P., and Young, J. A., Helix Waveguide, B.S.T.J., **35,** Nov. 1956, pp. 1347–1348.
2. Piefke, G., Wellenausbreitung in der Scheibenleitung, Arch. Elektr. Übertrag., **11,** 1957, pp. 49–59.
3. Katzenelenbaum, B. Z., Attenuation of H_{0n}-modes in a Helical Waveguide, Radioteknika i Elektronika, **4,** 1959, pp. 428–432.
4. Malin, W. W., and Siwow, A. N., The Theory of H_{01}-Wave Propagation in Helical Waveguide, Radioteknika i Elektronika, **4,** 1959, pp. 433–439.
5. Unger, H. G., Waveguides with Anisotropic Impedance Walls, Proc. Symposium on Electromagnetic Theory and Antennas, Copenhagen, 1962.
6. Unger, H. G., Winding Tolerances in Helix Waveguide, B.S.T.J., **40,** Mar. 1961, pp. 627–643.
7. King, A. P., and Mandeville, G. D., The Observed 33 to 90 kmc Attenuation of Two-Inch Improved Waveguide, B.S.T.J., **40,** Sept. 1961, pp. 1323–1330.
8. Unger, H. G., Wendelhohlleiter für sehr weite Frequenzbänder, Archiv Elektr. Übertr., **17,** 1963, pp. 359–369.
9. Routh, E. J., *Advanced Rigid Dynamics*, 6th Edition, London, 1905, pp. 461–467.
10. Meinke, H. H., Die Anwendung der konformen Abbildung auf Wellenfelder, Zeitschrift angew, Phys., **1** 1949, pp. 245–252.
11. Rice, S. O., Reflection from Corners in Rectangular Waveguides, Conformal Transformation, B.S.T.J., **28,** Jan., 1949, pp. 104–134.
12. Richmond, H. W., On the Electrostatic Field of a Plane or Circular Grating Formed of Thick Rounded Bars, Proc. London Math. Soc., Ser. 2, **22,** 1923, pp. 389–403.
13. Morrison, J. A., Heat Loss of Circular Electric Waves in Helix Waveguides, I.R.E. Trans. MTT-**6,** 1958, pp. 173-176.
14. Unger, H. G., Round Waveguide with Double Lining, B.S.T.J., **39,** Jan., 1960, pp. 161–167.
15. Morgan, S. P., Theory of Curved Circular Waveguide Containing an Inhomogeneous Dielectric, B.S.T.J., **36,** Sept., 1957, pp. 1209–1252.
16. Miller, S. E., Coupled Wave Theory and Waveguide Applications, B.S.T.J., **33,** May 1954, pp. 661–719.
17. Beck, A. C., and Rose, C. F. P., Waveguide for Circular Electric Mode Transmission, Proc. I.E.E., **106,** 1959, Pt.B., Supp. 13, p. 159.